No Evidence from FTIR Difference Spectroscopy That Glutamate-189 of the D1 Polypeptide Ligates a Mn Ion That Undergoes Oxidation during the S_0 to S_1, S_1 to S_2, or S_2 to S_3 Transitions in Photosystem II†

Melodie A. Strickler,‡ Warwick Hillier,§ and Richard J. Debus*,‡

Department of Biochemistry, University of California, Riverside, California 92521-0129, and Research School of Biological Sciences, Australian National University, G.P.O. Box 475, Canberra ACT, Australia 2601

Received March 24, 2006; Revised Manuscript Received May 23, 2006

ABSTRACT: In the recent X-ray crystallographic structural models of photosystem II, Glu189 of the D1 polypeptide is assigned as a ligand of the oxygen-evolving Mn_4 cluster. To determine if D1-Glu189 ligates a Mn ion that undergoes oxidation during one or more of the $S_0 \rightarrow S_1$, $S_1 \rightarrow S_2$, and $S_2 \rightarrow S_3$ transitions, the FTIR difference spectra of the individual S-state transitions in D1-E189Q and D1-E189R mutant PSII particles from the cyanobacterium *Synechocystis* sp. PCC 6803 were compared with those in wild-type PSII particles. Remarkably, the data show that neither mutation significantly alters the mid-frequency regions (1800−1200 cm^{-1}) of *any* of the FTIR difference spectra. Importantly, neither mutation eliminates any specific symmetric or asymmetric carboxylate stretching mode that might have been assigned to D1-Glu189. The small spectral alterations that *are* observed are similar in amplitude to those that are observed in wild-type PSII particles that have been exchanged into FTIR analysis buffer by different methods or those that are observed in D2-H189Q mutant PSII particles (the residue D2-His189 is located >25 Å from the Mn_4 cluster and accepts a hydrogen bond from Tyr Y_D). The absence of significant mutation-induced spectral alterations in the D1-Glu189 mutants shows that the oxidation of the Mn_4 cluster does not alter the frequencies of the carboxylate stretching modes of D1-Glu189 during the $S_0 \rightarrow S_1$, $S_1 \rightarrow S_2$, or $S_2 \rightarrow S_3$ transitions. One explanation of these data is that D1-Glu189 ligates a Mn ion that does not increase its charge or oxidation state during any of these S-state transitions. However, because the same conclusion was reached previously for D1-Asp170, and because the recent X-ray crystallographic structural models assign D1-Asp170 and D1-Glu189 as ligating different Mn ions, this explanation requires that (1) the extra positive charge that develops on the Mn_4 cluster during the $S_1 \rightarrow S_2$ transition be localized on the Mn ion that is ligated by the α-COO^- group of D1-Ala344 and (2) any increase in positive charge that develops on the Mn_4 cluster during the $S_0 \rightarrow S_1$ and $S_2 \rightarrow S_3$ transitions be localized on the one Mn ion that is *not* ligated by D1-Asp170, D1-Glu189, or D1-Ala344. An alternative explanation of the FTIR data is that D1-Glu189 does *not* ligate the Mn_4 cluster. This conclusion would be consistent with earlier spectroscopic analyses of D1-Glu189 mutants, but would require that the proximity of D1-Glu189 to manganese in the X-ray crystallographic structural models be an artifact of the radiation-induced reduction of the Mn_4 cluster that occurred during the collection of the X-ray diffraction data.

The catalytic site of water oxidation in photosystem II (PSII)[1] contains a cluster of four Mn ions and one Ca ion. The Mn_4 cluster accumulates oxidizing equivalents in response to light-induced electron-transfer reactions within PSII, thereby serving as the interface between one-electron photochemistry and the four-electron process of water oxidation (for reviews, see refs *1*−*4*). During each catalytic cycle, the Mn_4 cluster cycles through five oxidation states termed S_n, where "*n*" denotes the number of oxidizing equivalents that have been stored ($n = 0-4$). The S_1 state predominates in dark-adapted samples. Most interpretations of Mn-XANES data have concluded that the S_1 state consists of two Mn(III) and two Mn(IV) ions and that the S_2 state consists of one Mn(III) and three Mn(IV) ions (for reviews, see refs *5* and *6*). Whether the additional oxidizing equivalent

† Support for this work was provided by the National Science Foundation (Grant MCB 0111065 to R.J.D.) and by the National Institutes of Health (Grant GM66136 to R.J.D.). Additional support to W.H. was provided by the Human Frontiers Science Program (Grant No. RGP0029/2002).

* To whom correspondence should be addressed. Phone, (951) 827-3483; fax, (951) 827-4434, e-mail, richard.debus@ucr.edu.

‡ University of California.

§ Australian National University.

[1] Abbreviations: Chl, chlorophyll; EDTA, ethylenediaminetetraacetic acid; EPR, electron paramagnetic resonance; EXAFS, extended X-ray absorption fine structure; FTIR, Fourier transform infrared; MES, 2-(*N*-morpholino)-ethanesulfonic acid; NTA, nitrilotriacetic acid; P_{680}, chlorophyll species that serves as the light-induced electron donor in PSII; PSII, photosystem II; Q_A, primary plastoquinone electron acceptor; RH, relative humidity; WT(D1), wild-type control strain of *Synechocystis* sp. PCC 6803 that was constructed in identical fashion as the D1-Glu189 mutants but that contains the wild-type *psb*A-2 gene; WT(D2), wild-type control strain of *Synechocystis* sp. PCC 6803 that was constructed in identical fashion as the D2-H189Q mutant but that contains the wild-type *psbD*-1 gene; XANES, X-ray absorption near-edge structure; Y_Z, tyrosine residue that mediates electron transfer between the Mn cluster and $P_{680}^{+\bullet}$, Y_D, second tyrosine residue that can rapidly reduce $P_{680}^{+\bullet}$ in PSII.

10.1021/bi060583a CCC: $33.50
Published on Web 06/30/2006

of the S_3 state is localized on a Mn ion (*7*, *8*) or on a Mn ligand (*9*, *10*) remains in dispute. The S_4 state is a transient intermediate that reverts to the S_0 state with the concomitant release of O_2.

The amino acid residues that ligate the Mn_4 cluster are provided mainly by the D1 polypeptide, one of the core subunits of PSII. This ligation environment was predicted on the basis of spectroscopic analyses of site-directed mutants (for review, see ref *11*) and has been largely confirmed by recent X-ray crystallographic studies (*12*, *13*). In the recent ~3.5 Å (*12*) and ~3.0 Å (*13*) X-ray crystallographic structural models, the electron density that corresponds to the Mn_4Ca cluster is double-lobed. A single Mn ion is located in the smaller lobe and is ligated by D1-Asp170 and D1-Glu333 (*12*, *13*). The remaining Mn ions and the Ca ion are located in the larger lobe, with the Mn ions being ligated by D1-Glu189, D1-His332, D1-Asp342, and CP43-Glu354 (*12*) or by D1-Glu189, D1-His332, D1-Glu333, D1-Asp342, the α-COO^- group of D1-Ala344, and CP43-Glu354 (*13*). In the ~3.5 Å structural model (*12*), most of the carboxylate metal ligands are unidentate. In the ~3.0 Å structural model (*13*), most of the carboxylate metal ligands bridge two metal ions. The differences between the two structural models are probably caused by differences in data quality, extent of radiation damage, and approach to interpreting the electron density.

A principal disagreement between the X-ray crystallographic structural models and the earlier studies of site-directed mutants concerns the role of D1-Glu189. Both of the X-ray crystallographic structural models assign this residue as ligating the same Mn ion that is ligated by D1-His332. In contrast, the authors of the mutagenesis studies concluded that D1-Glu189 does *not* ligate Mn. The reasons were that (1) D1-E189Q, D1-E189K, and D1-E189R cells are photoautotrophic and evolve O_2 at 70−80% the rate of wild-type cells (*14*); (2) D1-E189Q PSII particles exhibit normal S_1 and S_2 multiline EPR signals (*14*), exhibit normal kinetics of O_2 release, and exhibit normal kinetics of electron transfer from Y_Z to $P_{680}^{\bullet+}$ and from the Mn_4 cluster to $Y_Z^{\bullet}$ during the $S_1 \rightarrow S_2$, $S_2 \rightarrow S_3$, and $S_3 \rightarrow S_0$ transitions (*15*); (3) D1-E189K and D1-E189R PSII particles exhibit normal rates of electron transfer from Y_Z to $P_{680}^{\bullet+}$ and from the Mn_4 cluster to $Y_Z^{\bullet}$ during the $S_1 \rightarrow S_2$ and $S_2 \rightarrow S_3$ transitions (*15*); and (4) D1-E189D, D1-E189N, D1-E189H, D1-E189G, and D1-E189S PSII particles contain Mn_4 clusters that evolve no O_2, exhibit no S_1 or S_2 state multiline EPR signals, and are unable to advance beyond an altered $S_2Y_Z^{\bullet}$ state, as shown by the accumulation of narrow $S_2Y_Z^{\bullet}$ EPR signals under multiple turnover conditions (*14*). Because changing D1-Glu189 to Gln, Lys, and Arg produced little change in PSII function, whereas changing D1-Glu189 to Asp, Asn, His, Gly, and Ser eliminated advancement beyond the $S_2Y_Z^{\bullet}$ state, it was proposed (*14*−*16*) that D1-Glu189 participates in the network of hydrogen bonds that is believed to facilitate electron transfer from the Mn_4 cluster to $Y_Z^{\bullet}$ during the higher S-state transitions (*17*−*19*). This network is thought to be disrupted by inhibitory treatments that prevent advancement beyond the $S_2Y_Z^{\bullet}$ state (e.g., the addition of acetate or ammonia or the depletion of Ca^{2+} or Cl^-) (*17*−*19*) and was proposed to be similarly disrupted in the non-O_2-evolving D1-Glu189 mutants (*14*, *16*). It was proposed that this hydrogen bond network is maintained by Gln because of its hydrogen bonding characteristics and by Lys and Arg because of their flexibility and hydrogen bonding characteristics (*14*, *16*) and that this network compensates for the change in charge that is created when D1-Glu189 is changed to Gln, Lys, or Arg[2] (*15*).

How does one reconcile the mutagenesis and X-ray crystallographic studies? Either the conclusions of the mutagenesis studies are incorrect with respect to D1-Glu189, or the crystallographic structural models are incorrect with respect to the relative positions of D1-Glu189 and the Mn_4 cluster. The possibility that the crystallographic structural models contain significant inaccuracies has been raised by recent XANES and EXAFS studies of PSII single crystals (*21*) and PSII membrane multilayers (*22*). In both of these studies, the XANES data show that the X-ray doses that were used in the crystallographic studies to irradiate the PSII crystals would have caused a surprisingly rapid reduction of the Mn_4 cluster's oxidized Mn(III/IV) ions to their fully reduced Mn(II) states (*21*, *22*). The corresponding EXAFS data show that this radiation-induced reduction causes the cluster's structural characteristics to change from that of a $Mn_4(III_2,IV_2)$ oxo-bridged Mn_4 complex to that of mononuclear hexaquo Mn(II) ions (*21*, *22*). Consequently, the diffraction data on which the structural models are based undoubtedly correspond to heterogeneous mixtures of damaged Mn clusters and hexaquo Mn(II) ions, with the former having disrupted μ-oxo bridges and altered Mn-ligand interactions (*21*, *22*). The extent that the structural models of the Mn_4 cluster and its ligation environment are distorted from the native structure remains to be determined.

To reinvestigate the possibility that D1-Glu189 ligates the Mn_4 cluster, and to determine if D1-Glu189 ligates a Mn ion that undergoes oxidation during one or more of the $S_0 \rightarrow S_1$, $S_1 \rightarrow S_2$, and $S_2 \rightarrow S_3$ transitions, we have compared the FTIR difference spectra of the individual S-state transitions in D1-E189Q and D1-E189R mutant PSII particles from the cyanobacterium *Synechocystis* sp. PCC 6803 with those in wild-type PSII particles. A large number of vibrational modes in PSII undergo shifts in frequency during individual S-state transitions. Many of these shifts produce strikingly large features in specific S_{n+1}-*minus*-S_n FTIR difference spectra, and many are clearly attributable to frequency shifts of carboxylate residues (*23*−*33*). The identification of these modes will complement X-ray crystallography by providing information about the dynamic structural changes that accompany water oxidation. Few of these modes have yet been identified (*31*, *33*−*35*). We recently employed isotopic labeling to identify the symmetric carboxylate stretching mode of the α-COO^- group of D1-Ala344 in the S_2-*minus*-S_1 FTIR difference spectra of wild-type PSII particles containing Ca or Sr (*34*, *35*) [also see ref *31*]. The frequency of this mode in the S_1 state and its ~17 or ~36 cm^{-1} downshift in the S_2 state imply that this group is a unidentate

[2] To explain the photoautotrophic growth of the mutants D1-E189L and D1-E189I, it has been proposed (*14*) that the relative bulk and hydrophobicity of Leu and Ile cause structural perturbations that permit the missing D1-Glu189 carboxylate group to be replaced by another residue or by a water molecule. The same explanation was advanced earlier (*20*) to account for the ability of D1-D170V cells to grow photoautotrophically and the ability of D1-D170L and D1-D170I cells to evolve O_2 despite the apparent role of D1-Asp170 as a ligand to Mn.

ligand of a Mn ion whose charge increases during the $S_1 \rightarrow S_2$ transition (*31*, *34*, *35*). A similar identification of one of the carboxylate stretching modes of D1-Glu189 in any of the $S_n \rightarrow S_{n+1}$ transitions could provide unequivocal spectroscopic evidence for the ligation of the Mn_4 cluster by D1-Glu189 and could provide information about the type of carboxylate ligation and the environment of the carboxylate group. If D1-Glu189 is the ligand of a Mn ion whose charge increases during a specific $S_n \rightarrow S_{n+1}$ transition, the increased charge should weaken the ligating Mn−O bond(s), thereby decreasing the frequency of the D1-Glu189 symmetric carboxylate stretching mode and possibly shifting the frequency of the D1-Glu189 asymmetric carboxylate stretching mode. The shifted mode(s) should appear in the corresponding S_{n+1}-*minus*-S_n FTIR difference spectrum of wild-type PSII particles but *not* in the spectra of D1-E189Q or D1-E189R PSII particles because the mutation has eliminated the carboxylate group. The absence of the mode in the mutant would permit its identification in the wild-type control.

However, the introduction of any site-directed mutation into a protein may also introduce structural perturbations outside the immediate vicinity of the mutation site because the mutation may alter multiple hydrogen bonds, perturb the conformation of the polypeptide backbone, or alter long-range electrostatic interactions. To gain some understanding of the likely magnitude of the indirect structural perturbations that may be associated with the D1-Glu189 mutations, we also examined (1) an unrelated mutation at a site far removed from the Mn_4 cluster (i.e., the mutation D2-H189Q) and (2) wild-type PSII particles that had been exchanged into the same FTIR analysis buffer by two different methods. The D2-H189Q mutation was chosen because (1) tyrosine Y_D forms a hydrogen bond with D2-His189 (*36*, *37*), and the replacement of this residue with Gln, Leu, or other residues decreases the light-dependent yield of $Y_D^{\bullet}$ (*38*, *39*) and alters the $Y_D^{\bullet}$ radical's EPR signal (*38*−*40*), probably by altering the orientation of the radical's aromatic ring (*16*, *41*) and (2) the elimination of $Y_D^{\bullet}$ alters both the spectral properties of $P_{680}^{\bullet+}$ (*42*) and the rates of electron transfer from Y_Z to $P_{680}^{\bullet+}$ (*42*, *43*) and from $Q_A^{\bullet-}$ to $Y_Z^{\bullet}$ (*44*), probably because of the loss of the electrostatic interaction between $Y_D^{\bullet}$ and P_{680} that was identified in a recent computational analysis of the ∼3.5 Å X-ray crystallographic structural model (*45*). Consequently, the mutation D2-H189Q can be expected to produce nonlocalized structural perturbations that may extend to the Mn_4 cluster. However, because D2-His189 is located >25 Å from the Mn_4 cluster (*12*, *13*), the D2-H189Q mutation cannot directly change the ligation of the Mn_4 cluster. Therefore, alterations to the S_{n+1}-*minus*-S_n FTIR difference spectra in D2-H189Q PSII particles can be attributed to indirect, mutation-induced structural perturbations. Similarly, spectral differences between wild-type samples that have been exchanged from purification/storage buffer into the same FTIR analysis buffer by two different methods do not reflect changes in metal ligation and should serve to mimic indirect, mutation-induced structural perturbations.

Our data show that the mid-frequency (1800−1200 cm^{-1}) S_1-*minus*-S_0, S_2-*minus*-S_1, S_3-*minus*-S_2, and S_0-*minus*-S_3 FTIR difference spectra of D1-E189Q and D1-E189R PSII particles are remarkably similar to those of wild-type PSII particles. The minor differences between the D1-Glu189 mutant and wild-type spectra are similar in amplitude to those in D2-H189Q PSII particles or in wild-type PSII particles that have been exchanged into the same FTIR analysis buffer by different methods. Importantly, neither D1-Glu189 mutation (neither D1-E189Q nor D1-E189R) eliminates any carboxylate modes from any of the difference spectra. The simplest explanations for these data are either (1) the Mn ion that is ligated by D1-Glu189 does not change its charge or oxidation state during the $S_0 \rightarrow S_1$, $S_1 \rightarrow S_2$, or $S_2 \rightarrow S_3$ transitions, or (2) D1-Glu189 does not ligate the Mn_4 cluster. Recently, the mid- and low-frequency S_2-*minus*-S_1 FTIR spectra of D1-E189Q PSII particles from *Synechocystis* sp. PCC 6803 were reported by another laboratory (*46*). Our mid-frequency S_2-*minus*-S_1 FTIR difference spectra resemble theirs. Our conclusions, however, are entirely different.

MATERIALS AND METHODS

Construction of Site-Directed Mutants and Propagation of Cultures. The D1-E189Q and D1-E189R mutations were constructed in the *psbA-2* gene of *Synechocystis* sp. PCC 6803 (*47*) and transformed into a host strain of *Synechocystis* that lacks all three *psbA* genes and contains a hexahistidine-tag (His-tag) fused to the C-terminus of CP47 (*48*). Single colonies were selected for ability to grow on solid media containing 5 μg/mL kanamycin monosulfate. The control WT(D1) strain was constructed in an identical fashion, except that the transforming plasmid carried no site-directed mutation. The designation "WT(D1)" differentiates this strain from the native wild-type strain that contains all three *psbA* genes, lacks a His-tag on the C-terminus of CP47, and is sensitive to antibiotics.

The D2-H189Q mutation was constructed in the *psbD-1* gene of *Synechocystis* sp. PCC 6803 (*49*) and transformed into a host strain of *Synechocystis* that lacks both *psbD* genes and contains a hexahistidine-tag (His-tag) fused to the C-terminus of CP47 (*48*). Single colonies were also selected for ability to grow on solid media containing 5 μg/mL kanamycin monosulfate. The control WT(D2) strain was constructed in an identical fashion, except that the transforming plasmid carried no site-directed mutation. The designation "WT(D2)" differentiates this strain from the native wild-type strain that contains both *psbD* genes, lacks a His-tag on the C-terminus of CP47, and is sensitive to antibiotics.

Cells were propagated as described previously (*32*, *34*, *35*). To verify the integrity of the mutant cultures that were harvested for the purification of PSII particles, an aliquot of each culture was set aside, and the complete sequence of the *psbA-2* or *psbD-1* gene was obtained after PCR amplification of purified genomic DNA (*47*).

Purification of PSII Particles. Isolated PSII particles were purified under dim green light at 4 °C with Ni−NTA superflow affinity resin (Qiagen, Valentia, CA) as described previously (*35*). Purified PSII particles [in purification buffer consisting of 1.2 M betaine, 10% (v/v) glycerol, 50 mM MES−NaOH (pH 6.0), 20 mM $CaCl_2$, 5 mM $MgCl_2$, 50 mM histidine, 1 mM EDTA, and 0.03% (w/v) *n*-dodecyl β-D-maltoside] were concentrated to ∼1.0 mg of Chl/mL by ultrafiltration, frozen in liquid N_2, and stored at −196 °C (vapor phase nitrogen).

FTIR Measurements. All manipulations were conducted under dim green light at 4 °C. For one set of wild-type

samples [WT(D1b) in Figure 1], approximately 30 μg of Chl was transferred into FTIR analysis buffer [40 mM sucrose, 10 mM MES−NaOH (pH 6.0), 5 mM $CaCl_2$, 5 mM NaCl, 0.06% (w/v) *n*-dodecyl β-D-maltoside (*28*, *32*)] by repeated concentration/dilution cycles as described previously (*35*). For all other samples, 60−80 μg of Chl was transferred into FTIR analysis buffer by passage through a 0.7 mL centrifugal gel filtration column [Micro Bio-Spin P-6 (Bio-Rad Laboratories, Hercules, CA)[3]]. The centrifuge (model 5417C with A8-11 Swing-Bucket rotor, Eppendorf, Inc., Westbury, NY) was operated at very low speed (27*g*). The sample was then concentrated to approximately 10 μL in a Microcon-100 concentrator in a standard microcentrifuge. Concentrated samples were immediately mixed with 1/10 volume of fresh 100 mM potassium ferricyanide (dissolved in water) and spread to a diameter of about 10 mm on a 15 mm diameter BaF_2 window. Samples were dried lightly (until tacky) under a stream of dry nitrogen gas. To maintain the humidity of the sample in the FTIR cryostat at 99% RH (*25*), 1 μL of 20% (v/v) glycerol (in water) was spotted onto the window, adjacent to the sample, but not touching it. A second IR window with a Teflon spacer (0.5 mm thick) was placed over the first and sealed in place with silicon-free high-vacuum grease (*25*). The sample was immediately loaded into the FTIR cryostat and allowed to equilibrate to 273.0 K in darkness for 2 h. The sample concentration and thickness were adjusted so that the absolute absorbance of the amide I band at 1657 cm^{-1} was 0.7−1.1.

FTIR Spectra. Mid-frequency FTIR spectra were recorded with a Bruker Equinox 55 spectrometer (Bruker Optics, Billerica, MA) as described previously (*32*). The spectral resolution for all spectra was 4 cm^{-1}. Samples were illuminated with flashes (~20 mJ/flash, ~7 ns fwhm) from a frequency-doubled Q-switched Nd:YAG laser [Surelite I (Continuum, Santa Clara, CA)]. After dark-adaptation, one pre-flash was applied followed by 5 min of additional dark-adaptation. This treatment was employed to oxidize Y_D and to maximize the proportion of centers in the S_1 state. Six successive flashes then were applied with an interval of 12.2 s between each. Two single-beam spectra were recorded before the first flash and one single-beam spectrum was recorded starting 0.33 s after the first and subsequent flashes (each single-beam spectrum consisted of 100 scans). The 0.33 s delay was incorporated to allow for the oxidation of Q_A^- by the ferricyanide. To obtain difference spectra corresponding to successive S-state transitions, the single-beam spectrum that was recorded after the *n*th flash was divided by the single-beam spectrum that was recorded immediately before the *n*th flash, and the ratio was converted to units of absorption. To estimate the background noise level, the second pre-flash, single-beam spectrum was divided by the first, and the ratio was converted to units of absorption. The sample was dark-adapted for 30 min, then the entire cycle was repeated, including the pre-flash and the 5 min additional dark-adaptation period. The entire cycle was repeated 12 times for each sample, and the difference spectra recorded with several samples were averaged.

[3] The Micro Bio-Spin P-6 is a polyacrylamide-based gel filtration column. Equivalent results were obtained with dextran-based Microspin G-25 gel filtration columns (Amersham Bioscience, Piscataway, NY).

Other Procedures. Chlorophyll concentrations and light-saturated rates of O_2 evolution were measured as described previously (*34*).

RESULTS

The O_2 evolving activities of the purified D1-E189Q, D1-E189R, and D2-H189Q PSII particles were 3.3−3.8, 3.0−4.0, and 2.1−2.6 mmol O_2 (mg of Chl)$^{-1}$ h^{-1}, respectively, compared to 5.1−5.5 mmol O_2 (mg of Chl)$^{-1}$ h^{-1} for WT(D1) and WT(D2) PSII particles. The lower O_2 evolving activity of PSII in the D1-E189Q and D1-E189R mutants (60−70% compared to wild-type) has been noted previously (*14*, *15*, *46*). Similarly, the lower O_2 evolving activity of PSII in the D2-H189Q mutant (40−50% compared to wild-type) has been noted previously (*39*, *50*).

The mid-frequency FTIR difference spectra of WT(D1), D1-E189Q, and D1-E189R PSII particles that were induced by four successive flash illuminations are compared in Figure 1 (panels A−D, traces *a*). The spectra that were induced by the first, second, third, and fourth flashes correspond predominantly to the S_2-*minus*-S_1, S_3-*minus*-S_2, S_0-*minus*-S_3, and S_1-*minus*-S_0 FTIR difference spectra, respectively. In each panel, two WT(D1) spectra are shown. The spectra labeled "WT(D1a)" correspond to WT(D1) samples that were exchanged into FTIR analysis buffer by passage through a centrifugal gel filtration column. The D1-E189Q and D1-E189R samples were exchanged into FTIR analysis buffer by the same method. The spectra labeled "WT(D1b)" correspond to WT(D1) samples that were exchanged into FTIR analysis buffer by repeated concentration/dilution cycles, as in ref *35*.

The mid-frequency FTIR difference spectra of WT(D1), WT(D2), and D2-H189Q PSII particles that were induced by four successive flash illuminations are compared in Figure 2. All of the samples in Figure 2 were exchanged into FTIR analysis buffer by passage through a centrifugal gel filtration column. The WT(D1a) data in this figure are reproduced from Figure 1.

All of the WT(D1a), WT(D1b), and WT(D2) S_{n+1}-*minus*-S_n FTIR difference spectra that are shown in Figures 1 and 2 resemble those that have been reported previously for wild-type *Synechocystis* sp. PCC 6803 PSII particles (*28*, *31*−*33*). Nevertheless, the WT(D1a) and WT(D1b) spectra show subtle differences between 1700 and 1300 cm^{-1} (Figure 1A−D, traces *a*). These differences are clearly evident in the double-difference spectra, WT(D1a)-*minus*-WT(D1b), that are shown in parts *c* of Figure 1A−D. Some of the largest differences appear between 1550 and 1500 cm^{-1} in the $\nu_{asym}(COO^-)$ region and between 1430 and 1370 cm^{-1} in the $\nu_{sym}(COO^-)$ region in the S_3-*minus*-S_2 spectra (Figure 1B, trace *c*). In contrast, the S_{n+1}-*minus*-S_n FTIR difference spectra of WT(D2) PSII particles more closely resembles the corresponding spectra of WT(D1a) PSII particles (Figure 2A−D, traces *a*). A comparison of the double-difference spectra, WT(D1a)-*minus*-WT(D2), and WT(D1a)-*minus*-WT(D1b) (Figure 2A−D, traces *c*) shows that the minor differences between the WT(D1a) and WT(D2) spectra are found primarily in the amide I region near 1650 cm^{-1} and in the amide II region near 1550 cm^{-1}.

The differences between the S_{n+1}-*minus*-S_n FTIR difference spectra of the WT(D1a) and WT(D1b) samples do not

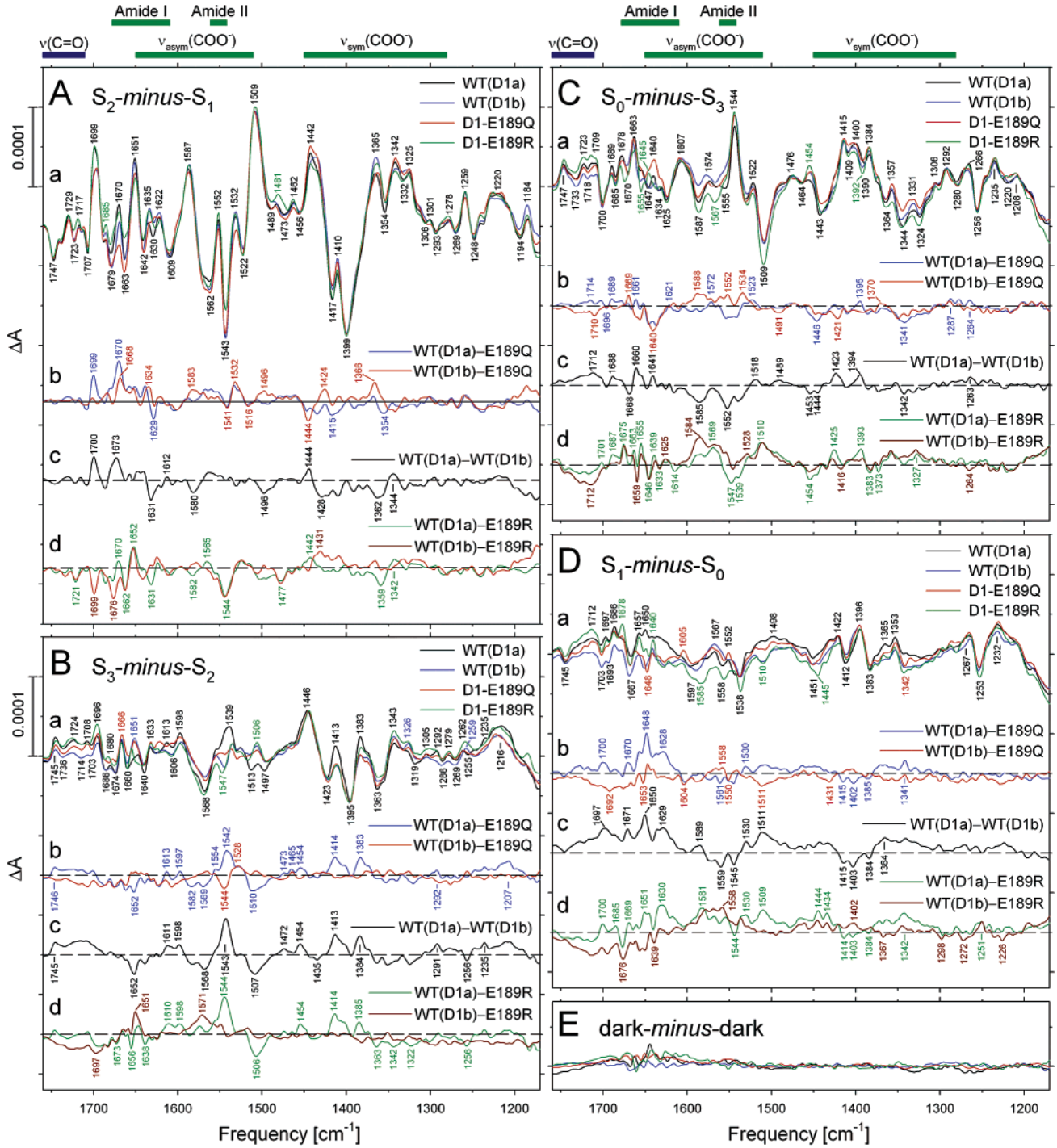

FIGURE 1: Comparison of the mid-frequency FTIR difference spectra of wild-type, D1-E189Q, and D1-E189R PSII particles in response to the first (A), second (B), third (C), and fourth (D) of six successive flash illuminations applied at 273 K [traces (*a*) in each panel]. The spectra (plotted from 1760 to 1170 cm^{-1}) correspond predominantly to S_2-*minus*-S_1, S_3-*minus*-S_2, S_0-*minus*-S_3, and S_1-*minus*-S_0 FTIR difference spectra, respectively. Spectra of two wild-type samples [WT(D1a) and WT(D1b)] are shown in each panel. The WT(D1a), D1-E189Q, and D1-E189R samples were exchanged into FTIR analysis buffer by passage through a centrifugal gel filtration column, while the WT(D1b) sample was exchanged by repeated concentration/dilution cycles (see text for details). To facilitate comparisons, the D1-E189Q and D1-E189R spectra have been multiplied by factors of ~1.4 and ~1.1, respectively, to maximize overlap with the wild-type spectra. Double-difference spectra (*b*, *c*, *d* in each panel) were calculated by directly subtracting the normalized traces shown in spectra *a*. The horizontal dashed lines indicate the zero levels. (E) Dark-*minus*-dark control traces of the WT(D1a), WT(D1b), D1-E189Q, and D1-E189R PSII particles are included to show the noise levels. The color coding in panel E is the same as in spectra *a* of panels A−D. Each spectrum represents the averages from nine samples (10 800 scans).

correspond to differences between PSII preparations because these spectra correspond to the *same* PSII preparations that were exchanged into FTIR analysis buffer by two different methods. In contrast, the more similar WT(D1a) and WT(D2) spectra correspond to *different* PSII preparations (from different wild-type control strains), that were exchanged into FTIR analysis buffer by the *same* method. The differences between the WT(D1a) and WT(D1b) spectra do not correspond to substantial irreversible damage caused by one buffer exchange method because the similarity of the

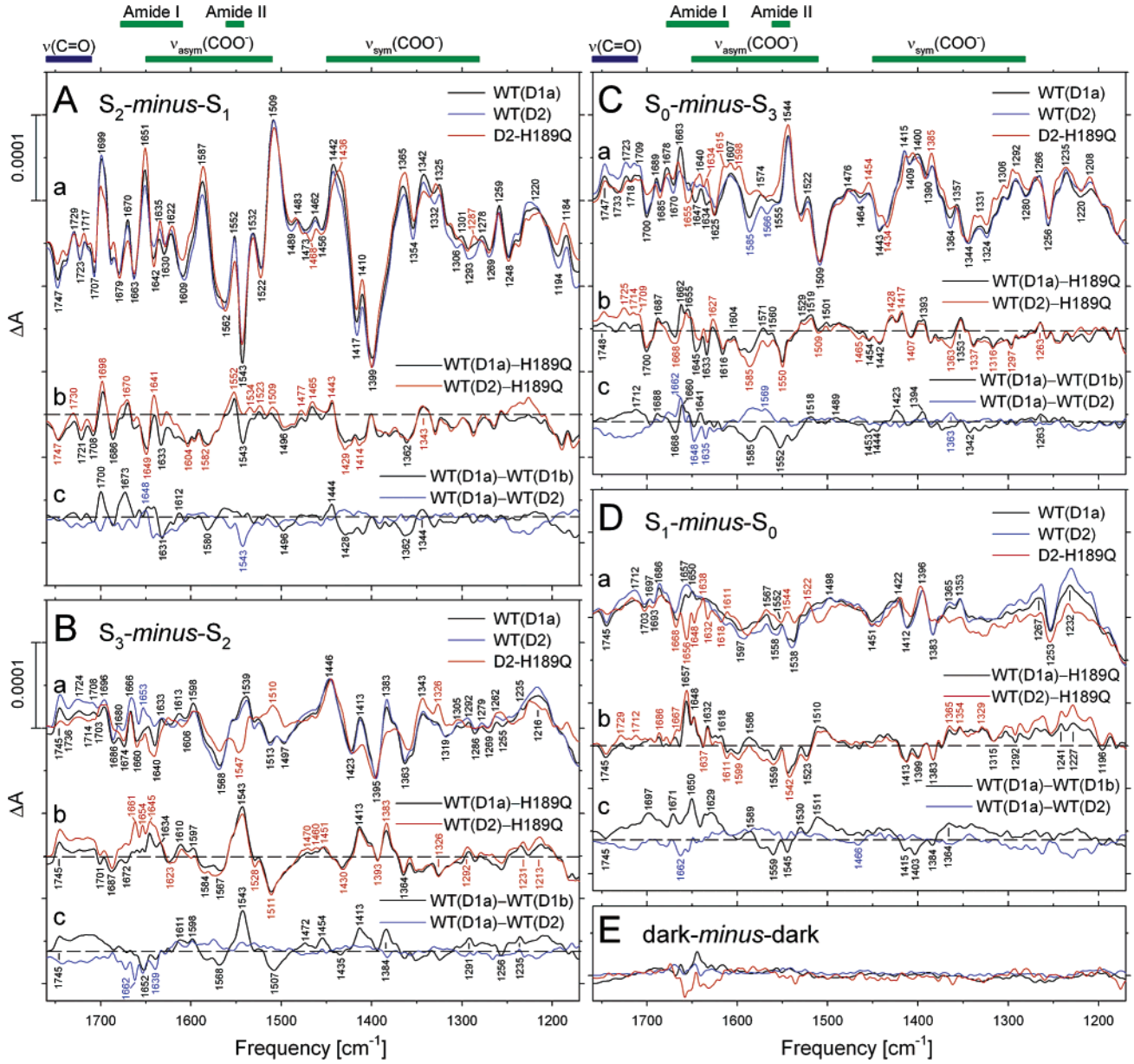

FIGURE 2: Comparison of the mid-frequency FTIR difference spectra of wild-type and D2-H189Q PSII particles in response to the first (A), second (B), third (C), and fourth (D) of six successive flash illuminations applied at 273 K [traces (*a*) in each panel]. The spectra (plotted from 1760 to 1170 cm^{-1}) correspond predominantly to S_2-*minus*-S_1, S_3-*minus*-S_2, S_0-*minus*-S_3, and S_1-*minus*-S_0 FTIR difference spectra, respectively. Spectra of two wild-type samples [WT(D1a) and WT(D2)] are shown in each panel. The mutant and both wild-type samples were exchanged into FTIR analysis buffer by passage through a centrifugal gel filtration column (see text for details). The WT-(D1a) spectra are reproduced from Figure 1. To facilitate comparisons, the D2-H189Q spectrum was multiplied by a factor of ~1.8 to maximize overlap with the wild-type spectra. Double-difference spectra (*b*, *c* in each panel) were calculated by directly subtracting the normalized traces shown in spectra *a*, except that the WT(D1a)-*minus*-WT(D1b) double-difference spectra in (*c*) are reproduced from Figure 1. The horizontal dashed lines indicate the zero levels. (E) Dark-*minus*-dark control traces of the WT(D1a), WT(D2), and D2-H189Q PSII particles are included to show the noise levels. The color coding in panel E is the same as in spectra *a* of panels A−D. Each wild-type spectrum represents the averages from nine samples (10 800 scans). The D1-H189Q spectrum represents the average from 10 samples (12 000 scans).

$\nu_{sym}(COO^-)$ regions of the S_0-*minus*-S_3 spectra (Figure 1C, trace *a*) implies that the miss-hit parameters are not substantially different in the WT(D1a) and WT(D1b) samples, meaning that the efficiencies of the S-state transitions are similar [the $\nu_{sym}(COO^-)$ region is particularly sensitive to an increase in the miss-hit parameter (*25*)]. It is evident that exchanging PSII samples into a buffer optimized for FTIR difference spectroscopy can induce minor structural perturbations in wild-type PSII particles that do not appreciably alter the functionality of the Mn_4 cluster.

A comparison of the normalized WT(D1a), WT(D1b), and D1-Glu189 mutant spectra (Figure 1A−D, traces *a*) shows that the D1-E189Q and D1-E189R S_{n+1}-*minus*-S_n FTIR difference spectra are remarkably similar to the corresponding wild-type FTIR difference spectra. Indeed, the features that are present in the WT(D1a)-*minus*-E189Q, WT(D1b)-*minus*-E189Q, WT(D1a)-*minus*-E189R, and WT(D1b)-*minus*-E189R double-difference spectra (Figure 1A−D, traces *b* and *d*) are similar in amplitude to the features that are present in the WT(D1a)-*minus*-WT(D1b) double-difference spectra

(Figure 1A−D, traces *c*). Note that there are few spectral features common to the WT(D1a)-*minus*-E189Q and WT-(D1b)-*minus*-E189Q double-difference spectra and few features common to the WT(D1a)-*minus*-E189R and WT(D1b)-*minus*-E189R double-difference spectra for any of the S_{n+1}-*minus*-S_n difference spectra. Indeed, there are few similarities between any of the WT-*minus*-E189Q and WT-*minus*-E189R double-difference spectra: the D1-E189Q and D1-E189R mutations produce different spectral alterations and neither eliminates a symmetric or asymmetric carboxylate stretching mode.

A comparison of the normalized WT(D1a), WT(D2), and D2-H189Q spectra (Figure 2A−D, traces *a*) shows that the D2-H189Q S_{n+1}-*minus*-S_n FTIR difference spectra are also very similar to the corresponding wild-type FTIR difference spectra. The features that are present in the WT(D1a)-*minus*-H189Q and WT(D2)-*minus*-H189Q double-difference spectra (Figure 2A−D, traces *b*) are similar in amplitude to the features that are present in the WT(D1a)-*minus*-WT(D1b) double-difference spectra (Figure 2A−D, traces *c*).

DISCUSSION

Providing controls for indirect mutation-induced structural perturbations should be an important aspect of analyzing proteins that contain site-directed mutations. This is especially true when the analyses include an analytical tool like FTIR difference spectroscopy that is highly sensitive to very small changes in structure. The D1-E189Q and D1-E189R mutations will introduce structural perturbations into PSII irrespective of whether D1-Glu189 ligates the Mn_4 cluster; the charges and chemical properties of Gln and Arg differ considerably from those of the native Glu residue. If D1-Glu189 does *not* ligate the Mn_4 cluster, these mutation-induced structural perturbations may be transmitted to the Mn_4 cluster *indirectly* by mutation-induced changes in hydrogen bonds, polypeptide backbone conformations, or long-range electrostatic interactions. Therefore, we sought to estimate the magnitudes of the structural perturbations that might be transmitted *indirectly* to the Mn_4 cluster by the D1-E189Q and D1-E189R mutations. To our knowledge, there have been no previous attempts to employ FTIR difference spectroscopy to assess the magnitudes of such indirect mutation-induced structural perturbations in any system. Our approach was to compare the S_{n+1}-*minus*-S_n FTIR difference spectra of D1-E189Q and D1-E189R PSII particles with the corresponding spectra of D2-H189Q PSII particles and with the corresponding spectra of two wild-type control samples that had been exchanged from purification/storage buffer into the same FTIR analysis buffer by two different methods. On the basis of these comparisons, we conclude that the small and relatively minor spectral differences that are observed between the wild-type and D1-Glu189 mutant S_{n+1}-*minus*-S_n FTIR difference spectra arise from indirect mutation-induced structural perturbations rather than from the loss of a metal-ligating D1-Glu189 carboxylate group. We base this conclusion on the following four observations.

First, the small amplitudes of the features in the WT-*minus*-E189Q and WT-*minus*-E189R double-difference spectra (Figure 1A−D, traces *b* and *d*) are similar to the correspondingly small features in the WT-*minus*-H189Q double-difference spectra (Figure 2A−D, traces *b*). Because D2-His189 is located >25 Å from the Mn_4 cluster (*12*, *13*), the D2-H189Q mutation cannot change the ligation of the Mn_4 cluster. Therefore, the differences between the S_{n+1}-*minus*-S_n FTIR difference spectra of D2-H189Q and wild-type PSII particles shown in Figure 2A−D must correspond to structural perturbations in the environment of the Mn_4 cluster that are induced indirectly by the D2-H189Q mutation. Such nonlocalized structural perturbations were not unexpected because of the influence of D2-His189 on $Y_D^\bullet$ and the influence of $Y_D^\bullet$ on the spectral and electron-transfer properties of P_{680} and Y_Z (*42*, *43*, *45*). The similar amplitudes of the spectral features in the WT-*minus*-E189Q, WT-*minus*-E189R, and WT-*minus*-H189Q double-difference spectra are an indication that the minor differences between the wild-type and D1-E189Q or D1-E189R mutant FTIR difference spectra arise from indirect mutation-induced structural perturbations and not from changes in Mn ligation.

Second, our data show that sample handling procedures, such as different methods for exchanging wild-type PSII particles into the same FTIR analysis buffer, can introduce minor structural perturbations into the environment of the Mn_4 cluster that are manifested as small alterations to the FTIR difference spectra (Figure 1A−D, traces *c*). These minor structural perturbations cannot be caused by changes in Mn ligation and do not alter the apparent efficiency of the S-state transitions. Although we do not understand their precise nature, minor structural perturbations induced by sample handling undoubtedly account for the small differences between the FTIR difference spectra of PSII *from the same organism* that are recorded in different laboratories despite similar apparent efficiencies of S-state turnover [e.g., compare the spectra of wild-type PSII particles from *Synechocystis* sp. PCC 6803 in Figure 1 of ref *28* with the corresponding spectra in Figure 1 of this study, particularly in the regions near 1650 and 1550 cm^{-1} and between 1425 and 1380 cm^{-1} in the S_3-*minus*-S_2 FTIR difference spectra]. The buffer exchange experiment, therefore, serves as a useful means of mimicking indirect mutation-induced structural perturbations. Therefore, the similar amplitudes of the spectral features in the WT-*minus*-E189Q, WT-*minus*-E189R, and WT(D1a)-*minus*-WT(D1b) double-difference spectra are an additional indication that the minor differences between the wild-type and D1-E189Q or D1-E189R mutant FTIR difference spectra arise from indirect mutation-induced structural perturbations and not from changes in Mn ligation.

Third, there are few, if any, features that are common to the WT-*minus*-E189Q and WT-*minus*-E189R double-difference spectra for any of the S-state transitions. This lack of correspondence provides an additional indication that these features arise from indirect mutation-induced structural perturbations; the different structures, chemical properties, and charges of the Gln and Arg side chains would be expected to produce different structural perturbations in D1-E189Q and D1-E189R PSII particles, as is observed.

Fourth, and most importantly, our data show no indication that either D1-Glu189 mutation eliminates a specific symmetric or asymmetric carboxylate stretching mode from any of the S_{n+1}-*minus*-S_n FTIR difference spectra. If D1-Glu189 was indeed a ligand of a Mn ion and sensed the oxidation of the Mn_4 cluster during one or more of the S-state transitions, then replacing Glu with Arg or Gln should eliminate 1−2 specific carboxylate modes from one or more

of the S_{n+1}-*minus*-S_n FTIR difference spectra, replacing them with a combination of CNH, NH, and/or CO modes. The elimination of the carboxylate modes should occur in both mutants and should be as obvious as the [1-^{13}C]alanine-induced shift of the $\nu_{sym}(COO^-)$ mode of the α-COO^- group of D1-Ala344 in prior studies (*31*, *34*, *35*). Yet, no such elimination is observed (Figure 1A−D, traces *b* and *d*). Therefore, our data show that neither the symmetric nor the asymmetric carboxylate stretching mode of D1-Glu189 is altered significantly when the Mn_4 cluster is oxidized during the $S_0 \rightarrow S_1$, $S_1 \rightarrow S_2$, or $S_2 \rightarrow S_3$ transitions.[4]

Our data show, therefore, that (1) the carboxylate group of D1-Glu189 is not sensitive to the oxidation state of the Mn_4 cluster during the $S_0 \rightarrow S_1$, $S_1 \rightarrow S_2$, or $S_2 \rightarrow S_3$ transitions and (2) great care must be taken when interpreting small changes in FTIR difference spectra in proteins containing site-directed mutations. One explanation of our data is that D1-Glu189 ligates a Mn ion that does not increase its charge or formal oxidation state during any of the $S_0 \rightarrow S_1$, $S_1 \rightarrow S_2$, or $S_2 \rightarrow S_3$ transitions. However, this explanation presents some challenges. First, in both of the recent X-ray crystallographic structural models, D1-Glu189 ligates one of the Mn ions that is located in the Mn_3Ca portion of the Mn_4Ca cluster (*12*, *13*). If D1-Glu189 does indeed ligate one of these Mn ions, then its carboxylate group is insensitive to the Mn oxidations that must occur elsewhere in this portion of the Mn_4Ca cluster during the $S_0 \rightarrow S_1$, $S_1 \rightarrow S_2$, or $S_2 \rightarrow S_3$ transitions. Second, the same explanation was offered previously for D1-Asp170 to explain similar FTIR data that were obtained with D1-D170H mutant PSII particles (*32*). The recent X-ray crystallographic structural models assign D1-Asp170 and D1-Glu189 as ligands of different Mn ions [Mn4 and Mn1, respectively, in the 3.0 Å structural model (*13*)]. Consequently, if neither of these Mn ions increases its charge or oxidation state during the $S_1 \rightarrow S_2$ transition, then the extra positive charge that develops on the Mn_4 cluster during this transition must necessarily be localized, probably to a single Mn ion. However, this conclusion conflicts with a resonant inelastic X-ray scattering (RIXS) study, whose authors concluded that this extra charge is strongly delocalized over the Mn_4 cluster (*55*). Third, this explanation constrains the identity of the Mn ion(s) whose charge or formal oxidation state increase during the $S_0 \rightarrow S_1$ and $S_2 \rightarrow S_3$ transitions. Because the α-COO^- group of D1-Ala344 is ligated to a Mn ion whose charge increases during the $S_1 \rightarrow S_2$ transition (*31*, *34*, *35*), decreases during the $S_3 \rightarrow S_0$ transition (*31*), and remains unchanged during the $S_0 \rightarrow S_1$ and $S_2 \rightarrow S_3$ transitions (*31*) [Mn2 in the 3.0 Å structural model (*13*)], any increase in positive charge that develops on the Mn_4 cluster during the $S_0 \rightarrow S_1$ and $S_2 \rightarrow S_3$ transitions must necessarily be localized on the one Mn ion that is *not* ligated by D1-Asp170, D1-Glu189, or D1-Ala344 [Mn3 in the 3.0 Å structural model (*13*)]. We are currently testing this possibility by analyzing mutations of the residue CP43-Glu354, identified as a ligand of this Mn ion in the 3.0 Å structural model (*13*).

An alternate explanation for our data is that D1-Glu189 does *not* ligate a Mn ion. This conclusion would be consistent with the earlier spectroscopic analyses of D1-Glu189 mutants (*14*, *15*, *20*), but presents another challenge: it requires that the proximity of D1-Glu189 to Mn in the X-ray crystallographic structural models be an artifact of the radiation-induced reduction of the Mn_4 cluster that occurred during the collection of the X-ray diffraction data. However, as noted earlier, recent X-ray absorption studies of PSII single crystals (*21*) and PSII membrane multilayers (*22*) show that the X-ray doses that were used in the crystallographic studies to irradiate the PSII crystals would have caused a surprisingly rapid reduction of the Mn_4 cluster's oxidized Mn(III/IV) ions to their fully reduced Mn(II) states and substantially modified the structure of the Mn_4 cluster. The extent that the current structural models reflect this radiation damage remains to be determined.

In the recent X-ray crystallographic structural models, D1-Glu189 is either located near (*12*) or identified as a possible ligand (*13*) of the Ca ion. The coordination of Ca by D1-Glu189 would be consistent with both our FTIR data, and the earlier mutagenesis studies, if replacing D1-Glu189 with residues other than Gln, Arg, or Lys (or Leu or Ile, see footnote 2), prevents advancement beyond the $S_2Y_Z^\bullet$ state by perturbing the network of hydrogen bonds that is believed (*17*−*19*) to facilitate electron transfer from the Mn_4 cluster to $Y_Z^\bullet$ during the higher S-state transitions. The Ca ion is believed to form part of this network (*56*, *57*), and its ligation by D1-Glu189 was proposed previously on the basis of spectroscopic analyses of Ca-depleted PSII preparations (*56*). It is noteworthy that D1-E189Q cells do not grow photoautotrophically in media having Sr substituted for Ca (R.J.D., unpublished results).

Recently, another group reported that the D1-E189Q mutation in *Synechocystis* sp. PCC 6803 causes specific changes to the $\nu_{sym}(COO^-)$ region in the mid-frequency S_2-*minus*-S_1 FTIR difference spectrum and between 640 and 570 cm^{-1} in the low-frequency S_2-*minus*-S_1 FTIR difference spectrum (*46*). The authors proposed that these spectral changes provide evidence for the ligation of Mn by D1-Glu189 (*46*). These data were obtained at 250 K. We have obtained similar mid-frequency wild-type and D1-E189Q S_2-*minus*-S_1 FTIR difference spectra at this temperature (*a* in Figure S1, Supporting Information). Our spectra differ slightly from theirs, especially in the amide I and amide II regions [e.g., the bands at 1633(+) and 1543(−) cm^{-1} are more intense in our spectra and the band at 1661(−) cm^{-1} is less intense]. In addition, the D1-E189Q mutation induces a smaller upshift of the ∼1436 cm^{-1} band in our spectrum. These spectral differences provide further evidence that sample handling procedures can introduce minor structural perturbations into the environment of the Mn_4 cluster that have little apparent functional significance. The authors of ref *46* argue that the E189Q-induced spectral alterations do not reflect indirect structural perturbations because ^2H_2O/^1H_2O exchange alters neither the $\nu_{sym}(COO^-)$ region of the mid-frequency spectrum (*26*) nor the E189Q-altered bands in the low-frequency spectrum (*30*). Their argument is that indirect structural perturbations would be transmitted through hydrogen bonds, and that, because the lack of ^2H_2O-induced

[4] The C═O carbonyl stretching modes of protonated carboxylate groups appear between 1760 and 1710 cm^{-1} (*51*, *52*). Because our data show no significant changes in this region of the S_{n+1}-*minus*-S_n, FTIR difference spectra in the D1-Glu189 mutants (Figure 1), and because our data show that neither carboxylate stretching mode of D1-Glu189 changes significantly during the $S_0 \rightarrow S_1$, $S_1 \rightarrow S_2$, or $S_2 \rightarrow S_3$ transitions, our data provide no support for a recent proposal (*53*, *54*) that D1-Glu189 changes its protonation state during the $S_1 \rightarrow S_2$ transition.

spectral alterations shows that the functional groups in question are not strongly hydrogen bonded, indirect structural perturbations could not be transmitted to these groups. However, this argument is weak because indirect structural perturbations could also be transmitted by alterations to polypeptide backbone conformations or electrostatic interactions. The amplitudes of the features in the mid-frequency WT-*minus*-E189Q double-difference spectra at 250 K [Figure S1 (Supporting Information) of this study and Figure 4 of ref *46*] are similar to those obtained at 273 K for all of the S-state transitions (Figure 1 of this study). On the basis of the arguments outlined above, and with the key advantage of having analyzed all of the S_{n+1}-*minus*-S_n FTIR difference spectra, we conclude that these spectral features represent indirect structural perturbations that are induced by the D1-E189Q mutation and do not represent the loss of a Mn-ligating carboxylate group. Turning to the low-frequency FTIR data that are reported in ref *46*, the spectral changes that were observed between 640 and 570 cm^{-1} in the D1-E189Q PSII particles (*46*) resemble spectral changes that were observed previously in D1-D170H PSII particles (*58*) and in samples having Sr substituted for Ca (*59*). These changes were attributed to indirect structural perturbations of a single Mn−O−Mn cluster mode (*32*, *58*, *59*). Consequently, the spectral changes between 640 and 570 cm^{-1} that are induced by the D1-E189Q mutation likely have the same origin. We conclude that neither ref *46* nor our study provides any compelling evidence for the ligation of Mn by D1-Glu189.[5]

CONCLUDING REMARKS

The mid-frequency S_{n+1}-*minus*-S_n FTIR difference spectra of D1-E189Q and D1-E189R PSII particles are remarkably similar to those of wild-type PSII particles. In particular, there is no indication that either mutation eliminates any carboxylate modes. Therefore, either D1-Glu189 ligates a Mn ion that does not increase its charge or oxidation state during any of the $S_0 \rightarrow S_1$, $S_1 \rightarrow S_2$, or $S_2 \rightarrow S_3$ transitions or D1-Glu189 does not ligate the Mn_4 cluster. If D1-Glu189 *does* ligate the Mn_4 cluster, then the FTIR data provides a constraint on the identity of the Mn ion(s) whose charge or oxidation state increases during the $S_0 \rightarrow S_1$ and $S_2 \rightarrow S_3$ transitions.

The similarity of the spectral changes that were observed in D2-H189Q PSII particles and in the different samples of wild-type PSII particles to those that were observed in D1-E189Q and D1-E189R PSII particles demonstrates that care must be taken in interpreting small changes in the FTIR difference spectra of proteins that contain site-directed mutations.

ACKNOWLEDGMENT

We are grateful to Anh P. Nguyen for maintaining the wild-type and mutant cultures of *Synechocystis* sp. PCC 6803 and for purifying the thylakoid membranes that were used for purifying the PSII particles.

SUPPORTING INFORMATION AVAILABLE

A comparison of the flash-induced S_2-*minus*-S_1 FTIR difference spectra of D1-E189Q and wild-type PSII particles recorded at 250 K. This material is available free of charge via the Internet at http://pubs.acs.org.

REFERENCES

1. Goussias, C., Boussac, A., and Rutherford, A. W. (2002) Photosystem II and Photosynthetic Oxidation of Water: An Overview, *Philos. Trans. R. Soc. London, Ser. B 357*, 1369−1381.
2. Sauer, K., and Yachandra, V. K. (2004) The Water-Oxidation Complex in Photosynthesis, *Biochim. Biophys. Acta 1655*, 140−148.
3. Vrettos, J. S., and Brudvig, G. W. (2004) Oxygen Evolution, *Compr. Coord. Chem. II 8*, 507−547.
4. Hillier, W., and Messinger, J. (2005) Mechanism of Photosynthetic Oxygen Production, in *Photosystem II: The Light-Driven Water*: *Plastoquinone Oxidoreductase* (Wydrzynski, T., and Satoh, K., Eds.) pp 567−608, Springer, Dordrecht, The Netherlands.
5. Sauer, K., Yano, J., and Yachandra, V. K. (2005) X-ray Spectroscopy of the Mn_4Ca Cluster in the Water-Oxidation Complex of Photosystem II, *Photosynth. Res. 85*, 73−86.
6. Yachandra, V. K. (2005) The Catalytic Manganese Cluster: Organization of the Metal Ions, in *Photosystem II: The Light-Driven Water: Plastoquinone Oxidoreductase* (Wydrzynski, T., and Satoh, K., Eds.) pp 235−260, Springer, Dordrecht, The Netherlands.
7. Haumann, M., Müller, C., Liebisch, P., Iuzzolino, L., Dittmer, J., Grabolle, M., Neisius, T., Meyer-Klaucke, W., and Dau, H. (2005) Structural and Oxidation State Changes of the Photosystem II Manganese Complex in Four Transitions of the Water Oxidation Cycle ($S_0 \rightarrow S_1$, $S_1 \rightarrow S_2$, $S_2 \rightarrow S_3$, and $S_{3,4} \rightarrow S_0$) Characterized by X-ray Absorption Spectroscopy at 20 K and Room Temperature, *Biochemistry 44*, 1894−1908.
8. Haumann, M., Liebisch, P., Müller, C., Barra, M., Grabolle, M., and Dau, H. (2005) Photosynthetic O_2 Formation Tracked by Time-Resolved X-ray Experiments, *Science 310*, 1019−1021.
9. Roelofs, T. A., Liang, W., Latimer, M. J., Cinco, R. M., Rompel, A., Andrews, J. C., Sauer, K., Yachandra, V. K., and Klein, M. P. (1996) Oxidation States of the Manganese Cluster During the Flash-Induced S-state Cycle of the Photosynthetic Oxygen-Evolving Complex, *Proc. Natl. Acad. Sci. U.S.A. 93*, 3335−3340.
10. Messinger, J., Robblee, J. H., Bergmann, U., Fernandez, C., Glatzel, P., Visser, H., Cinco, R. M., McFarlane, K. L., Bellacchio, E., Pizarro, S. A., Cramer, S. P., Sauer, K., Klein, M. P., and Yachandra, V. K. (2001) Absence of Mn-Centered Oxidation in the $S_2 \rightarrow S_3$ Transition: Implications for the Mechanism of Photosynthetic Water Oxidation, *J. Am. Chem. Soc. 123*, 7804−7820.
11. Debus, R. J. (2005) The Catalytic Manganese Cluster: Protein Ligation, in *Photosystem II: The Light-Driven Water: Plastoquinone Oxidoreductase* (Wydrzynski, T., and Satoh, K., Eds.) pp 261−284, Springer, Dordrecht, The Netherlands.
12. Ferreira, K. N., Iverson, T. M., Maghlaoui, K., Barber, J., and Iwata, S. (2004) Architecture of the Photosynthetic Oxygen-Evolving Center, *Science 303*, 1831−1838.
13. Loll, B., Kern, J., Saenger, W., Zouni, A., and Biesiadka, J. (2005) Towards Complete Cofactor Arrangement in the 3.0 Å Resolution Structure of Photosystem II, *Nature 438*, 1040−1044.
14. Debus, R. J., Campbell, K. A., Pham, D. P., Hays, A.-M. A., and Britt, R. D. (2000) Glutamate 189 of the D1 Polypeptide Modulates the Magnetic and Redox Properties of the Manganese Cluster and Tyrosine Y_Z in Photosystem II, *Biochemistry 39*, 6275−6287.
15. Clausen, K., Winkler, S., Hays, A. M., Hundelt, M., Debus, R. J., and Junge, W. (2001) Photosynthetic Water Oxidation in *Synechocystis* sp PCC6803: Mutations D1-E189K, R and Q are Without Influence on Electron Transfer at the Donor Side of Photosystem II, *Biochim. Biophys. Acta 1506*, 224−235.
16. Debus, R. J. (2001) Amino Acid Residues that Modulate the Properties of Tyrosine Y_Z and the Manganese Cluster in the Water

[5] An unexplained discrepancy between ref *46* and an earlier study (*20*) concerns the apparent S_2/S_1 midpoint potential in D1-E189Q cells. In ref *46*, upshifted thermoluminescence glow curves were interpreted as showing a decrease of the S_2/S_1 midpoint potential, whereas, in the earlier study, substantially unaltered kinetics of charge recombination between $Q_A^\bullet$ and the S_2 state were interpreted as showing little change in the S_2/S_1 midpoint potential (*20*).

Oxidizing Complex of Photosystem II, *Biochim. Biophys. Acta 1503*, 164−186.
17. Szalai, V. A., and Brudvig, G. W. (1996) Reversible Binding of Nitric Oxide to Tyrosyl Radicals in Photosystem II. Nitric Oxide Quenches Formation of the S_3 EPR Signal Species in Acetate-Inhibited Photosystem II, *Biochemistry 35*, 15080−15087.
18. Tommos, C., and Babcock, G. T. (2000) Proton and Hydrogen Currents in Photosynthetic Water Oxidation, *Biochim. Biophys. Acta 1458*, 199−219.
19. Vrettos, J. S., and Brudvig, G. W. (2002) Water Oxidation Chemistry of Photosystem II, *Philos. Trans. R. Soc. London, Ser. B 357*, 1395−1405.
20. Chu, H.-A., Nguyen, A. P., and Debus, R. J. (1995) Amino Acid Residues that Influence the Binding of Manganese or Calcium to Photosystem II. 1. The Lumenal Inter-Helical Domains of the D1 Polypeptide, *Biochemistry 34*, 5839−5858.
21. Yano, J., Kern, J., Irrgang, K.-D., Latimer, M. J., Bergmann, U., Glatzel, P., Pushkar, Y., Biesiadka, J., Loll, B., Sauer, K., Messinger, J., Zouni, A., and Yachandra, V. K. (2005) X-ray Damage to the Mn_4Ca Complex in Single Crystals of Photosystem II: A Case Study for Metalloprotein Crystallography, *Proc. Natl. Acad. Sci. U.S.A. 102*, 12047−12052.
22. Grabolle, M., Haumann, M., Müller, C., Liebisch, P., and Dau, H. (2006) Rapid Loss of Structural Motifs in the Manganese Complex of Oxygenic Photosynthesis by X-ray Irradiation at 10−300 K, *J. Biol. Chem. 281*, 4580−4588.
23. Noguchi, T., and Sugiura, M. (2001) Flash-Induced Fourier Transform Infrared Detection of the Structural Changes during the S-State Cycle of the Oxygen-Evolving Complex in Photosystem II, *Biochemistry 40*, 1497−1502.
24. Hillier, W., and Babcock, G. T. (2001) S-State Dependent FTIR Difference Spectra for the Photosystem II Oxygen Evolving Complex, *Biochemistry 40*, 1503−1509.
25. Noguchi, T., and Sugiura, M. (2002) Flash-Induced FTIR Difference Spectra of the Water Oxidizing Complex in Moderately Hydrated Photosystem II Core Films: Effect of Hydration Extent on S-State Transitions, *Biochemistry 41*, 2322−2330.
26. Noguchi, T., and Sugiura, M. (2002) FTIR Detection of Water Reactions During the Flash-Induced S-State Cycle of the Photosynthetic Water-Oxidizing Complex, *Biochemistry 41*, 15706−15712.
27. Noguchi, T., and Sugiura, M. (2003) Analysis of Flash-Induced FTIR Difference Spectra of the S-State Cycle in the Photosynthetic Water-Oxidizing Complex by Uniform ^{15}N and ^{13}C Isotope Labeling, *Biochemistry 42*, 6035−6042.
28. Yamanari, T., Kimura, Y., Mizusawa, N., Ishii, A., and Ono, T.-A. (2004) Mid- to Low-Frequency Fourier Transform Infrared Spectra of S-State Cycle for Photosynthetic Water Oxidation in *Synechocystis* sp. PCC 6803, *Biochemistry 43*, 7479−7490.
29. Suzuki, H., Sugiura, M., and Noguchi, T. (2005) pH Dependence of the Flash-Induced S-State Transitions in the Oxygen-Evolving Center of Photosystem II from *Thermosynechococcus elongatus* as Revealed by Fourier Transform Infrared Spectroscopy, *Biochemistry 44*, 1708−1718.
30. Kimura, Y., Ishii, A., Yamanari, T., and Ono, T.-A. (2005) Water-Sensitive Low-Frequency Vibrations of Reaction Intermediates during S-State Cycling in Photosynthetic Water Oxidation, *Biochemistry 44*, 7613−7622.
31. Kimura, Y., Mizusawa, N., Yamanari, T., Ishii, A., and Ono, T.-A. (2005) Structural Changes of D1 C-terminal α-Carboxylate during S-State Cycling of Photosynthetic Oxygen Evolution, *J. Biol. Chem. 280*, 2078−2083.
32. Debus, R. J., Strickler, M. A., Walker, L. M., and Hillier, W. (2005) No Evidence from FTIR Difference Spectroscopy That Aspartate-170 of the D1 Polypeptide Ligates a Manganese Ion That Undergoes Oxidation during the S_0 to S_1, S_1 to S_2, or S_2 to S_3 Transitions in Photosystem II, *Biochemistry 44*, 1367−1374.
33. Kimura, Y., Mizusawa, N., Ishii, A., and Ono, T.-A. (2005) FTIR Detection of Structural Changes in a Histidine Ligand during S-State Cycling of Photosynthetic Oxygen-Evolving Complex, *Biochemistry 44*, 16072−16078.
34. Chu, H.-A., Hillier, W., and Debus, R. J. (2004) Evidence that the C−Terminus of the D1 Polypeptide is Ligated to the Manganese Ion that Undergoes Oxidation During the S_1 to S_2 Transition: An Isotope-Edited FTIR Study, *Biochemistry 43*, 3152−3166.
35. Strickler, M. A., Walker, L. M., Hillier, W., and Debus, R. J. (2005) Evidence from Biosynthetically Incorporated Strontium and FTIR Difference Spectroscopy that the C−Terminus of the D1 Polypeptide of Photosystem II Does Not Ligate Calcium, *Biochemistry 44*, 8571−8577.
36. Campbell, K. A., Peloquin, J. M., Diner, B. A., Tang, X. S., Chisholm, D. A., and Britt, R. D. (1997) The τ-Nitrogen of D2 Histidine 189 is the Hydrogen Bond Donor to the Tyrosine Radical Y_D• of Photosystem II, *J. Am. Chem. Soc. 119*, 4787−4788.
37. Hienerwadel, R., Boussac, A., Breton, J., Diner, B. A., and Berthomieu, C. (1997) Fourier Transform Infrared Difference Spectroscopy of Photosystem II Tyrosine D using Site-Directed Mutagenesis and Specific Isotope Labeling, *Biochemistry 36*, 14712−14723.
38. Tommos, C., Davidsson, L., Svensson, B., Madsen, C., Vermaas, W. F. J., and Styring, S. (1993) Modified EPR Spectra of the $Tyrosine_D$ Radical in Photosystem II in Site-Directed Mutants of *Synechocystis* sp. PCC 6803, *Biochemistry 32*, 5436−5441.
39. Tang, X.-S., Chisholm, D. A., Dismukes, G. C., Brudvig, G. W., and Diner, B. A. (1993) Spectroscopic Evidence from Site-Directed Mutants of *Synechocystis* PCC 6803 in Favor of a Close Interaction Between Histidine 189 and Redox-Active Tyrosine 160, Both of Polypeptide D2 of the Photosystem II Reaction Center, *Biochemistry 32*, 13742−13748.
40. Un, S., Tang, X.-S., and Diner, B. A. (1996) 245 GHz High-Field EPR Study of Tyrosine-D and Tyrosine Z in Mutants of Photosystem II, *Biochemistry 35*, 679−684.
41. Diner, B. A., and Britt, R. D. (2005) The Redox-Active Tyrosine Y_Z and Y_D, in *Photosystem II: The Light-Driven Water: Plastoquinone Oxidoreductase* (Wydrzynski, T., and Satoh, K., Eds.) pp 207−233, Springer, Dordrecht, The Netherlands.
42. Sugiura, M., Rappaport, F., Brettel, K., Noguchi, T., Rutherford, A. W., and Boussac, A. (2004) Site-Directed Mutagenesis of *Thermosynechococcus elongatus* Photosystem II: The O_2-Evolving Enzyme Lacking the Redox-Active Tyrosine D, *Biochemistry 43*, 13549−13563.
43. Jeans, C., Schilstra, M. J., Ray, N., Husain, S., Minagawa, J., Nugent, J. H. A., and Klug, D. R. (2002) Replacement of Tyrosine D with Phenylalanine Affects the Normal Proton-Transfer Pathways for the Reduction of $P680^+$ in Oxygen-Evolving Photosystem II Particles from *Chlamydomonas*, *Biochemistry 41*, 15754−15761.
44. Boerner, R. J., Bixby, K. A., Nguyen, A. P., Noren, G. H., Debus, R. J., and Barry, B. A. (1993) Removal of Stable Tyrosine Radical D^+ Affects the Structure or Redox Properties of Tyrosine Z in Manganese-Depleted Photosystem II Particles from *Synechocystis* 6803, *J. Biol. Chem. 268*, 1817−1823.
45. Ishikita, H., and Knapp, E.-W. (2006) Function of Redox-Active Tyrosine in Photosystem II, *Biophys. J. 90*, 3886−3896.
46. Kimura, Y., Mizusawa, N., Ishii, A., Nakazawa, S., and Ono, T.-A. (2005) Changes in Structural and Functional Properties of Oxygen-Evolving Complex Induced by Replacement of D1-Glutamate 189 with Glutamine in Photosystem II: Ligation of Glutamate 189 Carboxylate to the Manganese Cluster, *J. Biol. Chem. 280*, 37895−37900.
47. Chu, H.-A., Nguyen, A. P., and Debus, R. J. (1994) Site-Directed Photosystem II Mutants with Perturbed Oxygen Evolving Properties: 1. Instability or Inefficient Assembly of the Manganese Cluster in Vivo, *Biochemistry 33*, 6137−6149.
48. Debus, R. J., Campbell, K. A., Gregor, W., Li, Z.-L., Burnap, R. L., and Britt, R. D. (2001) Does Histidine 332 of the D1 Polypeptide Ligate the Manganese Cluster in Photosystem II? An Electron Spin−Echo Envelope Modulation Study, *Biochemistry 40*, 3690−3699.
49. Faller, P., Rutherford, A. W., and Debus, R. J. (2002) Tyrosine D Oxidation at Cryogenic Temperature in Photosystem II, *Biochemistry 41*, 12914−12920.
50. Kim, S., Liang, J., and Barry, B. A. (1997) Chemical Complementation Identifies a Proton Acceptor for Redox-Active Tyrosine D in Photosystem II, *Proc. Natl. Acad. Sci. U.S.A. 94*, 14406−14411.
51. Venyaminov, S. Yu., and Kalnin, N. N. (1990) Quantitative IR Spectrophotometry of Peptide Compounds in Water (H_2O) Solutions. 1. Spectral Parameters of Amino Acid Residue Absorption Bands, *Biopolymers 30*, 1243−1257.
52. Barth, A. (2000) The Infrared Absorption of Amino Acid Side Chains, *Prog. Biophys. Mol. Biol. 74*, 141−173.
53. Petrouleas, V., Koulougliotis, D., and Ioannidis, N. (2005) Trapping of Metalloradical Intermediates of the S-States at Liquid Helium Temperatures. Overview of the Phenomenology and Mechanistic Implications, *Biochemistry 44*, 6723−6728.

54. Ioannidis, N., Zahariou, G., and Petrouleas, V. (2006) Trapping of the S_2 to S_3 State Intermediate of the Oxygen-Evolving Complex of Photosystem II, *Biochemistry 45*, 6252−6259.
55. Glatzel, P., Bergmann, U., Yano, J., Visser, H., Robblee, J. H., Gu, W., De Groot, F. M. F., Christou, G., Pecoraro, V. L., Cramer, S. P., and Yachandra, V. K. (2004) The Electronic Structure of Mn in Oxides, Coordination Complexes, and the Oxygen-Evolving Complex of Photosystem II Studied by Resonant Inelastic X-ray Scattering, *J. Am. Chem. Soc. 126*, 9946−9959.
56. Haumann, M., and Junge, W. (1999) Evidence for Impaired Hydrogen-Bonding of Tyrosine Y_Z in Calcium-Depleted Photosystem II, *Biochim. Biophys. Acta 1411*, 121−133.
57. Styring, S., Feyziyev, Y., Mamedov, F., Hillier, W., and Babcock, G. T. (2003) pH Dependence of the Donor Side Reactions in Ca^{2+}-Depleted Photosystem II, *Biochemistry 42*, 6185−6192.
58. Chu, H.-A., Debus, R. J., and Babcock, G. T. (2001) D1-Asp170 is Structurally Coupled to the Oxygen Evolving Complex in Photosystem II as Revealed by Light-Induced Fourier Transform Infrared Difference Spectroscopy, *Biochemistry 40*, 2312−2316.
59. Chu, H.-A., Sackett, H., and Babcock, G. T. (2000) Identification of a Mn−O−Mn Cluster Vibrational Mode of the Oxygen-Evolving Complex in Photosystem II by Low-Frequency FTIR Spectroscopy, *Biochemistry 39*, 14371−14376.

BI060583A